Mon. Not. R. Astron. Soc. **000**, 000–000 (0000) Printed 5 February 2008 (MN LATEX style file v2.2)

Detection of the Irradiated Donor in the LMXBs 4U 1636-536 (=V801 Ara) and 4U 1735-444 (=V926 Sco)

J. Casares[1⋆], R. Cornelisse[1,2⋆], D. Steeghs[3⋆], P.A. Charles[2,4⋆], R.I. Hynes[5⋆], K. O'Brien[6⋆], T. E. Strohmayer[7⋆]

[1] *Instituto de Astrofísica de Canarias, 38200 La Laguna, Tenerife, Spain*
[2] *School of Physics & Astronomy, University of Southampton, Southampton, SO17 1BJ, UK*
[3] *Harvard-Smithsonian Center for Astrophysics, Cambridge, MA 02138, USA*
[4] *South African Astronomical Observatory, P.O. Box 9. Observatory 7935, South Africa*
[5] *Department of Physics and Astronomy, 202 Nicholson Hall, Lousiana State, Baton Rouge, L.A. 70803, USA*
[6] *European Southern Observatory, Casilla 19001, Santiago 19, Chile*
[7] *Laboratory for High Energy Astrophysics, NASA Goddard Space Flight Center, Greenbelt, MD 20771, USA*

5 February 2008

ABSTRACT

Phase-resolved VLT spectroscopy of the bursting Low Mass X-ray Binaries 4U 1636-536/V801 Ara and 4U 1735-444/V926 Sco is presented. Doppler images of the NIII λ4640 Bowen transition reveal compact spots which we attribute to fluorescent emission from the donor star and enable us to define a new set of *spectroscopic* ephemerides. We measure $K_{\rm em} = 277 \pm 22$ km s^{-1} and $K_{\rm em} = 226 \pm 22$ km s^{-1} from the NIII spots in V801 Ara and V926 Sco respectively which represent strict lower limits to the radial velocity semi-amplitude of the donor stars. Our new ephemerides provide confirmation that lightcurve maxima in V801 Ara and likely V926 Sco occur at superior conjunction of the donor star and hence photometric modulation is caused by the visibility of the X-ray heated donor. The velocities of HeII λ4686 and the broad Bowen blend are strongly modulated with the orbital period, with phasing supporting emission dominated by the disc bulge. In addition, a reanalysis of burst oscillations in V801 Ara, using our spectroscopic T_0, leads to $K_1 = 90 - 113$ km s^{-1}. We also estimate the $K-corrections$ for all possible disc flaring angles and present the first dynamical constraints on the masses of these X-ray bursters. These are $K_2 = 360 \pm 74$ km s^{-1}, $f(M) = 0.76 \pm 0.47$ M$_\odot$ and $q = 0.21 - 0.34$ for V801 Ara and $K_2 = 298 \pm 83$ km s^{-1}, $f(M) = 0.53 \pm 0.44$ M$_\odot$ and $q = 0.05 - 0.41$ for V926 Sco. Disc flaring angles $\alpha \geq 12^\circ$ and $q \simeq 0.26 - 0.34$ are favoured for V801 Ara whereas the lack of K_1 constraint for V926 Sco prevents tight constraints on this system. Although both binaries seem to have intermediate inclinations, the larger equivalent width of the narrrow NIII line in V801 Ara at phase 0.5 relative to phase 0 suggests that it has the higher inclination of the two.

Key words: stars: accretion, accretion discs – binaries: close – stars: individual: (V801 Ara; V926 Sco)– X-rays: binaries –

1 INTRODUCTION

Low mass X-ray binaries (LMXBs) are interacting binaries where a low mass donor transfers matter onto a neutron star or black hole. 4U 1636-536 (=V801 Ara) and 4U 1735-444 (=V926 Sco) are among the optically brighter members in the class of *persistent* LMXBs, characterized by $L_{\rm x} \simeq 10^{37-38}$ erg s^{-1} and blue spectra with weak high-excitation emission lines (mainly HeII λ4686 and the CIII/NIII Bowen blend at λ4640). They also share similar properties: they are both atoll sources (as based on the pattern traced in X-ray color-color diagrams, see e.g.Hasinger & van der Klis 1989) with frequent burst activity and short orbital periods (3.80 and 4.65 hrs respectively) revealed through optical photometry (Corbet et al. 1986, Pedersen et al. 1981). Their lightcurves display shallow sinusoidal modulations which have been interpreted as due to the geometrically varying visibility of the irradiated donor star (e.g. van Paradijs et al. 1988). Therefore, the photometric maxima supposedly define orbital phase 0.5 i.e. inferior conjunction of the compact object. Note, however, that this assumption requires confirmation because photometric maxima can sometimes be associated with asymmetries in the disc structure such as the visibility of

⋆ E-mail: jcv@iac.es (JC); cornelis@astro.soton.ac.uk (RC); dsteeghs@head.cfa.harvard.edu (DS); pac@saao.ac.za (PAC); rih@phys.lsu.edu (RIH); kobrien@eso.org (KOB); stroh@clarence.gsfc.nasa.gov (TES)

the irradiated inner disc bulge at phase ~ 0.3 (e.g. 4U 1822-371 Hellier & Mason 1989) or superhump activity (see Haswell et al. 2001).

Only a few spectroscopic studies have been presented on these two binaries up to now. For example, Smale & Corbet (1991) report H_α spectroscopy of V926 Sco showing that the line core is dominated by emission from the disc bulge or splash region where the gas stream interacts with the outer disc rim. On the other hand, Augusteijn et al. (1998) (A98 hereafter) present radial velocity curves of HeII λ4686 and the Bowen blend at λ4640 for both V926 Sco and V801 Ara. They conclude that these high excitation lines are also tracing the motion of the disc bulge.

V801 Ara is particularly remarkable since it is one of only 14 bursters where "burst oscillations" (i.e. nearly coherent high-frequency pulsations) have been detected during several thermonuclear X-ray bursts (Giles et al. 2002, G02 hereafter). Furthermore, a train of burst oscillations was also discovered in a 13 min interval during a "superburst", showing a frequency drift which has been interpreted as the orbital motion of the neutron star (Strohmayer & Markwardt 2002, SM02 hereafter). By fitting the frequency evolution with a circular orbit SM02 constrain the radial velocity amplitude of the neutron star to the range $90 < K_1 < 175$ km s^{-1}. These constraints on K_1 will be readdressed and improved in this paper. Further constraints on the system parameters and the component masses, however, require dynamical information on the donor star which, unfortunately, is normally overwhelmed by the optical emission from the X-ray irradiated disc.

A new indirect method to extract dynamical information from donor stars in persistent LMXBs was proposed by Steeghs & Casares (2002) (SC02 hereafter). They detected narrow high excitation emission lines from the irradiated surface of the donor star in Sco X-1 which led to the first determination of its radial velocity curve and mass function. These lines are strongest in the Bowen blend, a combination of C III and N III lines which are powered by photoionization and fluorescence (respectively) due to UV photons arising from the hot inner disk (McClintock et al. 1975). This technique has been amply confirmed by subsequent studies of the eclipsing ADC (Accretion Disc Corona) and X-ray pulsar 4U 1822-371 (Casares et al. 2003), the black hole soft X-ray transient GX 339-4 during its 2002 outburst (Hynes et al. 2003) and Aql X-1 during its 2004 outburst (Cornelisse et al. 2006).

In this paper we apply this method to the X-ray bursters 4U 1636-536 (=V801 Ara) and 4U 1735-444 (=V926 Sco) and present the first detection of the donor stars in these two LMXBs. The paper is organized as follows: Section 2 summarizes the observation details and data reduction. The average spectra and main emission line parameters are presented in Sect. 3, with multigaussian deconvolution of the Bowen blend. In Section 4 we analyse the radial velocities and orbital variability of the strong Bowen blend and HeII λ4686 emission lines. Estimates of the systemic velocities are obtained through the Double Gaussian technique applied to the wings of the HeII line. Using these systemic velocities we compute Doppler tomograms of HeII λ4686 and the Bowen fluorescence NIII λ4640 which are presented in Section 5. The NIII maps display evidence of irradiated emission from the donor star, which is used to refine the absolute phasing and systemic velocities. Finally, in Section 6 we provide an improved determination of K_1 for V801 Ara and present our constraints on the masses in the two binaries.

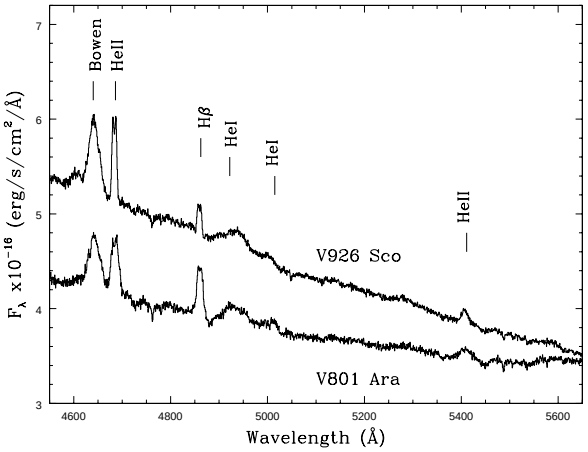

Figure 1. Summed spectra of V801 Ara and V926 Sco with the principal emission lines indicated.

2 OBSERVATIONS AND DATA REDUCTION

V801 Ara and V926 Sco were observed on the nights of 23 and 25 June 2003 using the FORS2 Spectrograph attached to the 8.2m Yepun Telescope (UT4) at the Observatorio Monte Paranal (ESO). A total of 42 spectra of 600s of V801 Ara and 102 exposures of 200s of V926 Sco were obtained with the R1400V holographic grating, covering a complete orbital cycle per night for each target. We used a 0.7 arcsec slit width which rendered a wavelength coverage of $\lambda\lambda$4514-5815 at 70 km s^{-1} (FWHM) resolution, as measured from Gaussian fits to the arc lines. The seeing was variable between 0.6" – 1.2" during our run. The flux standard Feige 110 was also observed with the same instrumental configuration to correct for the instrumental response of the detector.

The images were de-biased and flat-fielded, and the spectra subsequently extracted using conventional optimal extraction techniques in order to optimize the signal-to-noise ratio of the output spectra (Horne 1986). A He+Ne+Hg+Cd comparison lamp image was obtained in daytime to provide the wavelength calibration scale. This was obtained by a 4th-order polynomial fit to 19 lines, resulting in a dispersion of 0.64 Å pix^{-1} and rms scatter < 0.05 Å. Instrumental flexure was monitored through cross-correlation between the sky spectra and was found to be very small, always within 14 km s^{-1} (0.4 pix.) on each night. These velocity drifts were removed from each individual spectrum, and the zero point of the final wavelength scale was established from the position of the strong OI λ5577.338 sky line. All the spectra were calibrated in flux using observations of the flux standard Feige 110. However, due to light loss caused by our narrow slit and variable seeing conditions, our flux calibration is only accurate to $\sim 50\%$.

3 AVERAGE SPECTRA AND EMISSION LINE PARAMETERS

Figure 1 presents the average spectra of V801 Ara and V926 Sco in f_λ flux units. They show a blue continuum with broad high excitation emission lines of HeII λ4686, λ5411, the Bowen blend at $\lambda\lambda$4630-50 and Hβ, which are typical of X-ray active LMXBs. Possible HeI lines at λ4922 and λ5015 are also identified but these are significantly weaker. Table 1 summarizes the FWHM, EW and centroid λ_c of the main emission lines obtained through simple Gaussian fits. We note that the average spectra (including the

Table 1. Emission line Parameters

Line	*FWHM* (*km s*$^{-1}$)	*EW* (*Å*)	*Centroid* (*Å*)	ΔV (*km s*$^{-1}$)
V801 Ara				
Bowen	1848 ± 65	4.25 ± 0.03	4643.2 ± 0.4	–
HeII λ4686	1216 ± 45	3.31 ± 0.03	4685.6 ± 0.3	-9 ± 11
$H\beta$	963 ± 56	1.67 ± 0.02	4860.9 ± 0.3	-25 ± 21
V926 Sco				
Bowen	1662 ± 65	3.99 ± 0.02	4641.5 ± 0.4	–
HeII λ4686	657 ± 26	2.18 ± 0.02	4683.9 ± 0.2	-118 ± 12
$H\beta$	507 ± 39	0.43 ± 0.02	4859.2 ± 0.4	-134 ± 25

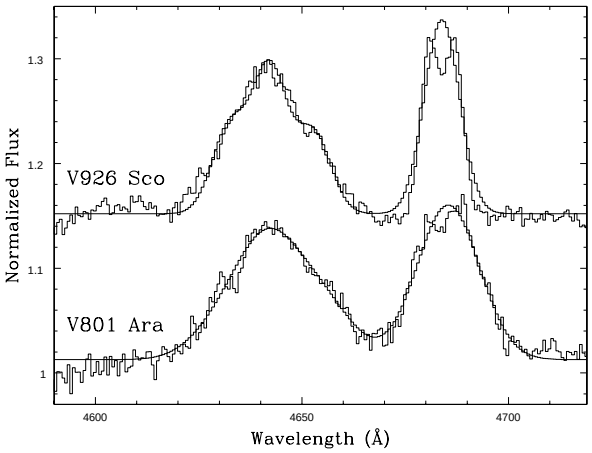

Figure 2. Combined fit to HeII λ4686 and the Bowen blend using three Gaussians at $\simeq$4634Å (NIII), $\simeq$4641Å (NIII) and $\simeq$4651Å (CIII). See text for details.

line strengths) look very similar to those presented by A98, which seems to imply that there has been no large, long-term variations between the two data epochs. Incidentally, the EWs and FWHMs of all lines do not show any significant nigh-to-night variability nor modulation with the orbital period. Aside from the intrinsically broad Bowen blend, which is a blend of at least three CIII/NIII transitions, we note that emission lines are a factor $\sim$2 narrower in V926 Sco than in V801 Ara. Given the similarities in their orbital periods, this suggests a projection effect with a lower inclination angle for V926 Sco. In addition, the emission line centroids in V926 Sco are significantly blueshifted, probably due to a larger (approaching) systemic velocity. This also applies to the Bowen complex since the difference in wavelength between V801 Ara and V926 Sco (-110 km/s) is consistent with the difference in velocities found for the other lines. The blue continuum is also steeper for V926 Sco, as expected because of its lower reddening (see A98).

The Bowen blend mainly consists of emissions corresponding to the NIII transitions at $\lambda\lambda$4634,4641,4642 and CIII at $\lambda\lambda$4647,4651,4652 (Schachter et al. 1989). In an attempt to estimate the relative contribution of the different transitions we have performed a combined multi-Gaussian fit to the average emission profiles of HeII λ4686 and the Bowen blend for the two LMXBs. The fit consists of four Gaussians, one for the HeII line, two for the NIII emissions at λ4634 and λ4641-2 and another for the CIII emissions at λ4647-52. Free parameters are the line widths, which are set to be equal for all the lines, individual line centroids and intensities. The line widths are mainly driven by the fit to the unblended HeII line and hence the latter is effectively used as a template to constrain the line profiles within the Bowen blend. Figure 2 presents the results of the fit. Because widths are set to be the same for all lines, flux ratios are given by simple peak ratios. Our best fit yields NIII ratio $I(\lambda 4634)/I(\lambda\lambda 4641-2) = 0.31 \pm 0.10$ and 0.59 ± 0.02 for V801 Ara and V926 Sco, respectively. This is a factor ≤ 2 lower than the theoretical NIII ratio of 0.71, computed by Nussbaumer (1971) for Bowen fluorescence, but consistent with the results of Schachter et al. (1989) for Sco X-1. Similarly, Hynes (private communication) finds a NIII ratio in the range 0.36-0.56 (depending on time) for GX 339-4 during its 2002 outburst. We can also calculate the CIII/NIII ratio $I(\lambda\lambda 4647-52)/I(\lambda 4634+\lambda\lambda 4641-2)$ and find 0.38 ± 0.06 and 0.35 ± 0.01 for V801 Ara and V926 Sco respectively. For comparison, we have performed the same analysis on average spectra of Sco X-1 and 4U 1822-371, using data presented in SC02 and Casares et al. (2003), and find 0.44 ± 0.03 and 0.49 ± 0.01 respectively. The lower CIII/NIII ratio in V801 Ara and V926 Sco may indicate possible evidence of CNO processed material but we have to be cautious here because of the oversimplification in our fitting model. In particular, we cannot rule out other possible transitions (most likely OII lines at λ4641.8 and λ4649.1; see McClintock et al. 1975) contributing to our components at $\sim$4641Å and $\sim$4651Å, which so far we have assumed to be dominated by NIII and CIII transitions. Furthermore, since the CIII and OII lines are not powered by Bowen fluorescence but photoionization, different line ratios may stem from differences in efficiency of these two excitation mechanisms rather than true CNO abundance variations.

4 RADIAL VELOCITY STUDY AND ORBITAL VARIABILITY

Figure 3 displays the radial velocities of the Bowen blend and HeII λ4686 line for V801 Ara and V926 Sco, obtained by cross-correlating the individual spectra with Gaussians of fixed FWHM as given in Table 1. We have assumed $\lambda_c = 4643.0$ for the central wavelength of the Bowen blend. The velocities are folded in orbital phase, using the ephemerides of G02 and A98 for V801 Ara and V926 Sco but shifted in phase by +0.5 to make phase zero coincide with the inferior conjunction of the donor star. These will be called the *photometric ephemerides* and will be used throughout this Section. The accumulated phase uncertainty at the time of our observations is ± 0.06 for both systems. Note that this phase convention assumes that lightcurve maxima are driven by the visibility of the irradiated donor star.

The radial velocity curves for V801 Ara show maxima at phase $\sim$ 1. This phasing suggests that the velocity variations contain a significant component arising in the disc bulge (which has its maximum visibility at phase $\sim$ 0.75), caused by the interaction of the gas stream with the outer edge of the disc, as is typically seen in persistent LMXBs (e.g. 4U 1822-371; Cowley, Crampton & Hutchings 1982). On the other hand, the radial velocity curves for V926 Sco show maxima at phase $\sim$ 0.7. By comparing the HeII curves in the two binaries we clearly see evidence for a large systemic velocity of $\sim$ -150 km s^{-1} in V926 Sco, in good agreement with Smale & Corbet (1991). We also note that the CIII/NIII blend in V801 Ara is modulated with a much larger amplitude than in V926 Sco i.e. 280 km s^{-1} versus 70 km s^{-1}, respectively.

Figure 4 presents the trailed spectra of the Bowen blend and

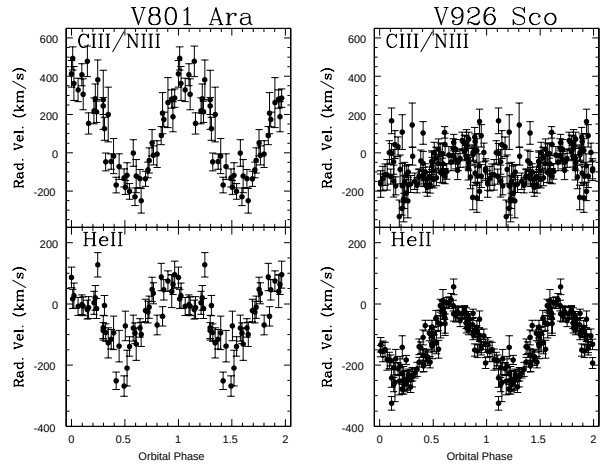

Figure 3. Radial velocity curves of the Bowen blend (top) and HeII λ4686 in V801 Ara and V926 Sco.

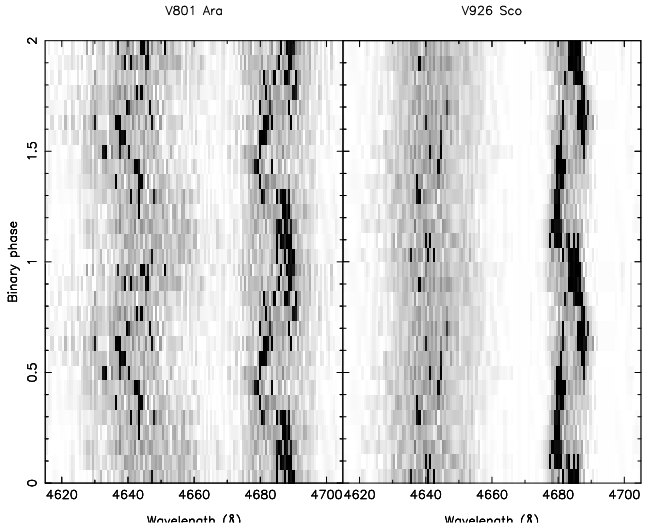

Figure 4. Trailed spectra showing the orbital evolution of the Bowen blend and HeII λ4686 in 15 phase bins using the *photometric ephemerides*

HeIIλ4686 for V801 Ara and V926 Sco, after co-adding our individual spectra in 15 phase bins to improve statistics. The core of the emission lines in V801 Ara show clear S-wave components. The S-wave in the Bowen blend is quite narrow and it may arise from the heated face of the donor star, as observed in Sco X-1 (SC02). The S-wave in HeII is rather extended and is likely produced in a region with a large velocity dispersion such as the disc bulge. On the other hand, the Bowen blend in V926 Sco is rather noisy and does not exhibit any clear components that are visible by eye. The HeII trailed spectra do show a clear orbital modulation with complex structure.

Following our work on Sco X-1 (SC02) and 4U 1822-371 (Casares et al. 2003), we have applied the double-Gaussian technique (Schneider & Young 1980) to the wings of the HeII λ4686 line in an attempt to estimate the radial velocity curve of the compact object. The trailed spectra presented in Fig. 4 demonstrate that the line cores are dominated by strong, complex, low-velocity components associated with asymmetric emission from the outer disc and/or the donor star, which we want to avoid. Therefore, by convolving the emission line with a double-Gaussian filter of sufficiently large Gaussian separation we can extract radial velocity curves from the wings of the profile, which are expected to follow the motion of the compact star. We have used a double-Gaussian bandpass with $FWHM = 100$ km s^{-1} and relative Gaussian separations in the range $a = 400 - 1400$ km s^{-1} in steps of 100 km s^{-1}. In order to improve statistics, we have co-added our spectra in 15 phase bins using the *photometric ephemerides*. The radial velocity curves obtained for different Gaussian separations are subsequently fitted with sine-waves of the form $V(\phi) = \gamma + K \sin 2\pi(\phi - \phi_0)$, fixing the period to the orbital value. The best fitting parameters are displayed as a function of the Gaussian separation a in a Diagnostic Diagram (see Fig. 5).

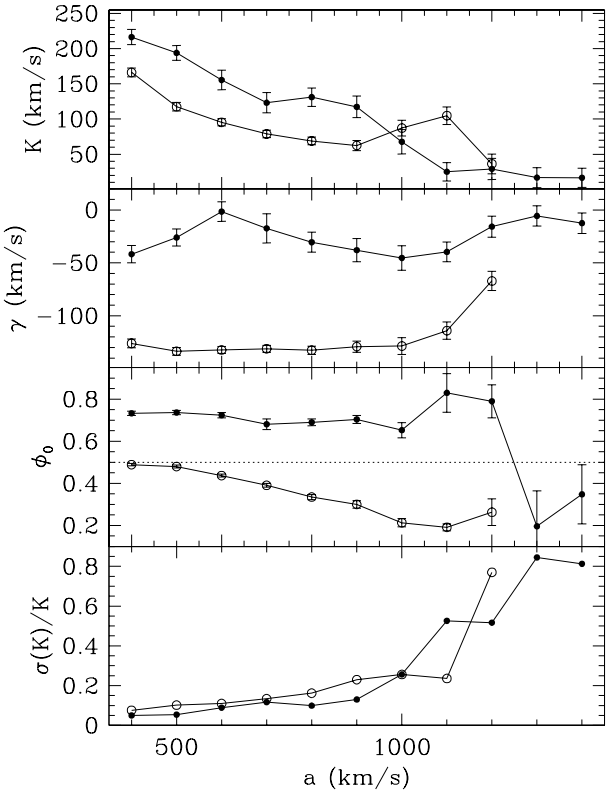

Figure 5. Diagnostic Diagram for HeII λ4686 in V801 Ara (solid circles) and V926 Sco (open circles). The dotted horizontal line marks $\phi_0 = 0.5$ or the expected inferior conjunction of the compact object, according to the *photometric ephemerides*.

In both cases we see how the line cores are dominated by high-amplitude ($K \sim 200$ km s^{-1}) S-waves which fade as we move to the line wings, where lower $K-$amplitudes of a few tens of km s^{-1} are found. On the other hand, the γ velocities are very steady throughout the profiles, with average values of ~ -30 (V801 Ara) and ~ -130 km s^{-1} (V926 Sco). The blue-to-red crossing phase for V926 Sco displays a smooth decreasing trend from the line core to the wings, whereas it is rather constant for V801 Ara, with an average value of $\phi_0 \sim 0.7$. We estimate that the velocity points start to be corrupted by continuum noise for Gaussian separations larger than $a \sim 1000$ as indicated by the diagnostic parameter $\sigma(K)/K$ (see Shafter et al. 1986). Therefore, we decided to adopt the average values for the parameters obtained from the last two separations before $\sigma(K)/K$ starts to rise i.e. $a = 900 - 1000$ km s^{-1} for V801 Ara and 1000-1100 km s^{-1} for V926 Sco. This yields $K_1 = 93 \pm 25$ km s^{-1}, $\gamma = -42 \pm 4$ km s^{-1}, $\phi_0 = 0.68 \pm 0.03$

for V801 Ara and $K_1 = 96 \pm 9$ km s^{-1}, $\gamma = -121 \pm 7$ km s^{-1}, $\phi_0 = 0.20 \pm 0.01$ for V926 Sco. The errorbars have been adjusted to incorporate the scatter between different values within our preferred range. Note that ϕ_0 of V801 Ara is delayed by ~ 0.18 with respect to the inferior conjunction of the compact object (dotted line in Fig. 5), as predicted by the *photometric ephemerides*. This is classically observed in interacting binaries and interpreted as contamination of the line wings by residual emission from the disc-bulge/hot-spot (Marsh 1998). On the other hand, ϕ_0 of V926 Sco leads the inferior conjunction of the compact star by ~ 0.30, according to the *photometric ephemerides*. Such a large shift is unexpected and a full discussion is diverted to Sect. 6. Furthermore, we also note the very asymmetric distributions obtained in the HeII Doppler maps (see next Sect.) which may invalidate the double-Gaussian technique. Therefore, the constraints on zero-phase, γ-velocity and K_1 (for V801 Ara) will be superseded in the following sections.

5 BOWEN FLUORESCENCE FROM THE IRRADIATED COMPANION

Doppler tomography enables us to map the brightness distribution of a binary system in velocity space through combining orbital phase spectra (see details in Marsh 2001). This is particularly effective when dealing with weak emission features which are barely detected or embedded by noise in individual spectra, such as our narrow Bowen emission lines. In order to compute Doppler images of the NIII λ4640 fluorescence line in V801 Ara and V926 Sco we have rectified the individual spectra by subtracting a low order spline fit to the continuum regions and rebinned them into a uniform velocity scale of 37 km s^{-1} per pixel. Doppler images were subsequently computed using the *photometric ephemerides* and $\gamma = -42$ and -121 km s^{-1} for V801 Ara and V926 Sco, respectively. The maps show compact spots shifted in phase by $+0.03$ and -0.18 with respect to the expected location of the donor star in the velocity maps (i.e. along the vertical V_y axis)[1]. Assuming that these spots are produced on the irradiated hemisphere of the donor star, as has been shown to be the case in Sco X-1 (SC02) and 4U 1822-371 (Casares et al. 2003), we correct the previous *photometric ephemerides* and derive the following *spectroscopic ephemerides*, which will be used in the remainder of the paper:

$$T_0(HJD) = 2452813.531(2) + 0.15804693(16)E \quad (1)$$

$$T_0(HJD) = 2452813.495(3) + 0.19383351(32)E \quad (2)$$

where the zero-phase error comes from the uncertainty in the centroid position of the spots. Equation (1) corresponds to the ephemerides of V801 Ara and equation (2) to V926 Sco. With these ephemerides, the HeII λ4686 maps of the two binaries show a crescent shape brightness distribution pointing towards emission from an extended disc bulge.

Following SC02 we have used the HeII Doppler maps to refine the systemic velocities derived in the previous section. The χ^2 value of the map was calculated for a range of γ's, and the best fit in terms of mimimal χ^2 was achieved for $\gamma \simeq -39$ km s^{-1} (V801 Ara) and $\gamma \simeq -132$ km s^{-1} (V926 Sco). The use of an incorrect systemic velocity has the effect of blurring bright spots into , as opposed to V801 Ara,elongated "defocused" features in Doppler images. Therefore, as a further test, we have also computed NIII λ4640 maps for a set of γ-velocities in the range -200 – +200 km s^{-1} and we looked for the best focused NIII spots by computing the skewness using box sizes of 5, 10 and 20 pixels. We find that the most symmetric and compact spots are found for γ values in the range -29 – -39 km s^{-1} (V801 Ara) and 137-143 km s^{-1} (V926 Sco). Therefore, we decided to adopt $\gamma = -34 \pm 5$ km s^{-1} (V801Ara) and $\gamma = -140 \pm 3$ km s^{-1} (V926 Sco) and these are the values that we have used in the final Doppler maps, which are presented in Fig. 6. The NIII maps reveal compact bright spots which we interpret as irradiated emission from the inner hemisphere of the donor star. These spots are obviously located along the vertical axis because of our ephemerides definition. We have calculated the position of these spots by computing their centroids using the centering algorithm CENTROID in IRAF[2] and find $K_{\rm em} = 277 \pm 22$ km s^{-1} (V801 Ara) and 226 ± 22 km s^{-1} (V926 Sco). We note that $K_{\rm em}$ is very weakly dependent on γ, with only a 10 km s^{-1} drift when γ varies by ± 20 km s^{-1} around our central value. Therefore, our $K_{\rm em}$ determinations seem very robust and they represent strict lower limits to the true radial velocity semiamplitude K_2 of the donor stars because they must arise from the irradiated hemisphere facing the neutron star. Further confirmation of our system

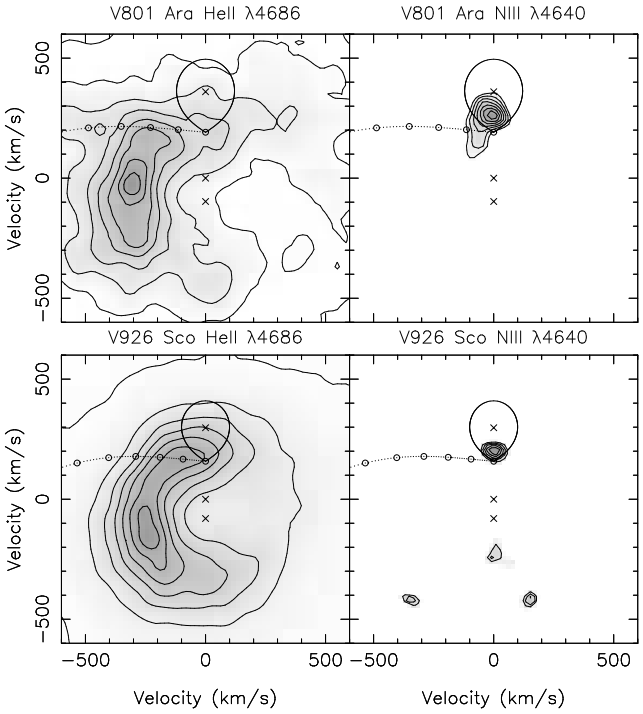

Figure 6. Doppler maps of HeII λ4686 (left panels) and NIII λ4640 (right panels) for V801 Ara and V926 Sco, computed using our *spectroscopic ephemerides*. Systemic velocities $\gamma = -34$ km s^{-1} and $\gamma = -140$ km s^{-1} were adopted for V801 Ara and V926 Sco, respectively. For comparison we also plot the gas stream trajectory (in units of 0.1 R$_L$1) and Roche lobe of the donor star for the case of $K_2 = 360$ km s^{-1} (V801 Ara) and $K_2 = 298$ km s^{-1} (V926 Sco). A mass ratio $q = 0.27$ has been assumed for the two binaries.

[1] Note that the greyscale in the NIII maps have been set to enhance the contrast of the sharp components. This is the reason why these maps do not show any trace of emission from the underlying broad component.

[2] IRAF is distributed by the National Optical Astronomy Observatories, which are operated by the Association of Universities of Research in Astronomy, Inc., under cooperative agreement with the Nacional Science Foundation.

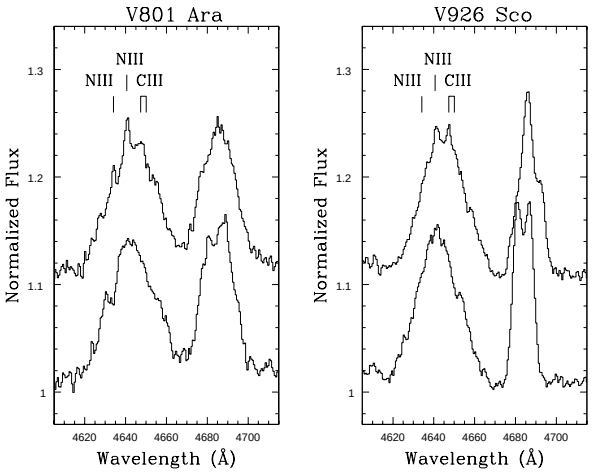

Figure 7. Average spectra of V801 Ara (left panel) and V926 Sco (right panel). Top spectra have been Doppler corrected in the rest frame of the donor using the spectroscopic ephemerides and the K-velocity amplitudes derived from the bright spots in the NIII $\lambda 4640$ Doppler images. The narrow NIII and CIII lines are clearly seen in the Bowen blend. These are smeared out and cannot be detected in the straight averages shown at bottom. Noise has been filtered using a 2 pixel boxcar smoothing.

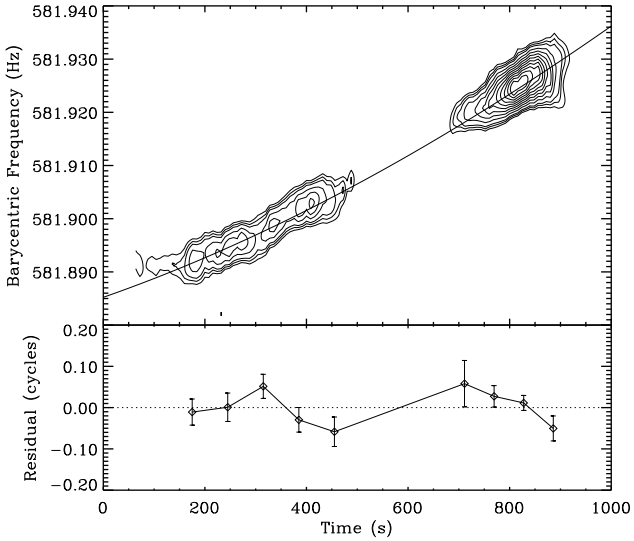

Figure 8. Top panel: Dynamic Fourier power contours showing the excursion in oscillation frequency during the 2001 February 22 superburst from 4U 1636-53 (V801 Ara) with the best fitting orbit model overlayed. Time zero for the x-axi is MJD 51962.7102530038 (TDB) Bottom panel: Pulse phase residuals for the best fitting model.

parameters is provided by the appearance of the sharp CIII/NIII transitions after coadding all the spectra in the rest frame of the NIII λ4640 emission line region (see Fig. 7). Note that we have not attempted to compute Doppler images of the Hβ lines because these are contaminated by phase-variable absorption components, as was also the case in 4U 1822-371 (e.g. Casares et al. 2003). Absorption violates the principles of Doppler Tomography and makes it very difficult to interpret the corresponding Doppler images.

6 DISCUSSION

The detection of NIII λ4640 fluorescence emission from the irradiated donor in V801 Ara and V926 Sco provides new absolute (spectroscopic) ephemerides and opens the possibility to derive the first constraints on the dynamical masses of these two LMXBs. In the light of the new ephemerides, the photometric lightcurve maxima of V801 Ara take place at phase 0.47 ± 0.06 (with the uncertainty dominated by error propagation of the G02 ephemerides) and, therefore, they are consistent with X-ray irradiation of the donor star. On the other hand, lightcurve maxima in V926 Sco are located at orbital phase 0.82 ± 0.06. This is in between the maximum visibility of the irradiated donor and the disc-bulge and hence it would imply that lightcurve maxima arise by a combination of these two emitting regions. However, we note that the uncertainty in the photometric ephemerides of V926 Sco is likely to be higher than stated in A98 due to the limited number of arrival times fitted and their large scatter (Augusteijn, private communication). Therefore, it is possible that lightcurve maxima in V926 Sco are also consistent with superior conjunction of the irradiated donor star. This is the most likely scenario because it would be hard to understand an emission source peaking at phase ~ 0.8 in an irradiation dominated environment without invoking some strange (and stable) disc configuration.

We have also determined the systemic velocities for the two binaries i.e. -34 ± 5 km s^{-1} (V801 Ara) and -140 ± 3 km s^{-1} (V926 Sco). These can be compared with $V_{\rm r}$, the radial velocity, relative to the Local Standard of Rest, due to Galactic rotation at the location of the binaries. For the case of V801 Ara, we take $l = 332.9^{\circ}$, $b = -4.8^{\circ}$ and $d = 6 - 7$ kpc, based on peak fluxes of radius-expansion X-ray bursts for $M_1 = 1.4 - 2$ M$_{\odot}$ (Galloway et al. 2005). Assuming the Galactic rotation curve of Nakanishi & Sofue (2003) we find $V_{\rm r}$ in the range -103 to -111 km s^{-1}. This is much larger than our systemic velocity which could be explained through the recoil velocity gained by the binary during the supernova explosion which formed the neutron star. Thus, we can set a lower limit to the kick velocity in V801 Ara of $\simeq 70$ km s^{-1}. Regarding V926 Sco, we take $l = 346.1^{\circ}$, $b = -7.0^{\circ}$ and a distance $d = 9.1$ kpc (for a canonical 1.4 M$_{\odot}$ neutron star, see A98). The Galactic rotation curve at the position of V926 Sco yields $V_{\rm r} = -111$ km s^{-1}, close but significantly lower than our systemic velocity. The difference might also be ascribed to a kick velocity received by the neutron star at birth or, alternatively, a neutron star mass of $\simeq$1.7 M$_{\odot}$. Note that the latter implies a larger distance of $d = 10$ kpc and hence $V_{\rm r} = -140$ km s^{-1}.

6.1 System Parameters for V801 Ara

The NIII λ4640 spot in the Doppler map yields $K_{\rm em} = 277 \pm 22$ km s^{-1}. It must arise on the inner hemisphere of the donor and hence it sets a lower limit to the velocity semi-amplitude of the companion's center of mass K_2. In order to find the real K_2 we need to calculate the $K - correction$ or $K_{\rm em}/K_2$ for the case of emission lines in illuminated atmospheres, which depends mainly on the binary mass ratio $q = M_2/M_1$ (with M_2, M_1 the masses of the donor and compact star respectively) and the disc flaring angle α. The $K - correction$ has been calculated by Muñoz-Darias, Casares & Martínez-Pais (2005) using an irradiation binary code which includes shadowing by an axisymmetric flared disc. The results are tabulated as a function of q, α and the inclination angle i in Table 1 of their paper, although the dependence on i is very weak. The $K - correction$ is constrained between $\alpha = 0$ (i.e. we neglect disc shadowing) and the geomet-

ric limit set by emission from the irradiated limb of the donor, i.e. $K_{\rm em}/K_2 < 1 - 0.213q^{2/3}(1+q)^{1/3}$ (see Muñoz-Darias et al. 2005).

An upper limit on q is established by taking $M_1 \geq 1.4{\rm M}_\odot$ and $M_2 \leq 0.48$ M$_\odot$, the largest possible zero-age main sequence (ZAMS) star fitting in a 3.79 hr period Roche lobe (Tout et al. 1996), which leads to $q \leq 0.34$. As a first approach, one can assume the empirical Mass-Radius relation for low-mass stars in cataclysmic variables and LMXBs (see e.g. Smith & Dhillon 1998, Warner 1995) which yields $M_2 \simeq 0.32$. This, combined with a canonical neutron star of $M_1 \simeq 1.4$ M$_\odot$, would lead to a plausible $q \sim 0.23$. The $K-correction$ for $K_{\rm em} = 277 \pm 22$ km s^{-1} and $q \sim 0.23$ would yield $303 < K_2 < 404$ km s^{-1}, where we have adopted the coefficients for the case $i = 40^\circ$ in Table 1 of Muñoz-Darias et al. (2005) because V801 Ara is not eclipsing.

A more refined $K-correction$ requires a knowledge of q. This can be constrained by the rotational broadening $V_{\rm rot}\sin i$ of the companion star which, for the case of synchronous rotation, is related to q through

$$V_{\rm rot}\sin i \simeq 0.462 K_2 q^{1/3}(1+q)^{2/3} \quad (3)$$

(Wade & Horne 1988). A lower limit to $V_{\rm rot}\sin i$ can be estimated from the width of the sharp NIII fluorescence emission in the Doppler corrected average spectrum. This is because emission lines arise not from the entire Roche lobe but from the irradiated part only. A multigaussian fit to the Bowen profile presented in Fig. 7 gives $FWHM(NIII\lambda4640) = 140 \pm 21$ km s^{-1}, which includes the effect of our intrinsic instrumental resolution (70 km s^{-1}). This has been accounted for by broadening a Gaussian template of $FWHM = 70$ km s^{-1} between 10 and 200 km s^{-1}, in steps of 10 km s^{-1}, using a Gray rotational profile (Gray 1992) without limb-darkening, because fluorescence lines arise in optically thin conditions. Our simulation indicates that $V_{\rm rot}\sin i = 92 \pm 16$ km s^{-1} is equivalent to $FWHM = 140 \pm 21$ km s^{-1}. On the other hand, by substituting $V_{\rm rot}\sin i \geq 76$ km s^{-1} and the $K-correction$ for $\alpha > 0^\circ$ into equation (3), one finds a secure lower limit $q \geq 0.08$.

An upper limit to the rotational broadening of the donor star is set by $V_{\rm rot}\sin i = 2\pi R_2 \sin i/P$. By assuming that the donor must be more evolved than a ZAMS star within a 3.79 hr Roche lobe, then $R_2 \leq 0.44 R_\odot$ (Tout et al. 1996). This, together with $i \leq 78^\circ$ (lack of X-ray eclipses for $q \geq 0.08$), yields $V_{\rm rot}\sin i \leq 138$ km s^{-1}.

Further constraints are provided by the study of burst oscillations which can set limits to the neutron star's projected velocity $K_1 (= qK_2)$. SM02 derived $90 \leq K_1 \leq 175$ km s^{-1} by fitting the frequency drift of highly coherent X-ray pulsations observed in an 800s interval during a superburst. They used a circular orbit model and fixed the zero phase to the ephemeris of G02. We have used our new spectroscopic ephemeris to reanalyse the superburst pulsation data in order to better constrain K_1. Based on our spectroscopic ephemeris, the pulsation interval during the superburst from V801 Ara comes slightly earlier in orbital phase by 0.032 cycles as compared to the G02 ephemeris. We fit the pulsation data (see SM02 for details on the phase timing analysis) to a circular orbit model with the reference epoch fixed to our new T_0, and we also fixed the orbital period (using the G02 value). This leaves two free parameters, the projected neutron star velocity, K_1, and the rest-frame spin frequency, ν_0. We find acceptable fits with a reference epoch within the $\pm1\sigma$ range for our spectroscopic T_0. The inferred K_1 velocity ranges from 90 - 113 km s^{-1} as T_0 ranges over $\pm1\sigma$. The best fit χ^2 values range from 14.6 to 10.6 (with 7 dof) over this same range, that is, higher velocities are modestly favored, but given the shortness of the pulse train compared to the orbital period, we do not consider these differences as significant. With the reference epoch fixed, the statistical error on the velocity is much smaller than the range given above, so 90 - 113 km s^{-1} is a robust range for K_1 at the $\pm1\sigma$ limits of T_0. The best fit ν_0 ranges from 582.04143 to 582.09548 Hz, and which may help constrain future searches for a persistent millisecond pulsar in V801 Ara. Figure 8 summarizes the results of the new timing analysis.

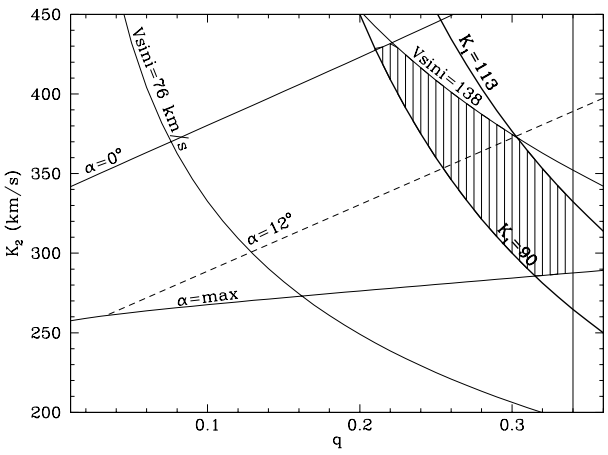

Figure 9. Constraints on K_2 and q for V801 Ara. The disc flaring angle must be between $\alpha = 0^\circ$ and $\alpha = max$, whereas the rotational broadening is constrained between the observed $V_{\rm rot}\sin i \simeq 76$ km s^{-1} and 138 km s^{-1}, the maximum allowed for a ZAMS star in a 3.8hr period and for $i \leq 78^\circ$. The shaded area represents the K_1 solution obtained from a reanalysis of the superburst pulsations. These constrain the binary mass ratio to be $q = 0.21 - 0.34$ and $K_2 = 286 - 433$ km s^{-1}. For comparison we also mark (dashed line) the solution for a hypothetic disc flaring angle of $\alpha = 12^\circ$.

Fig. 9 summarizes all our restrictions in the $K_2 - q$ parameter space i.e. $0^\circ \leq \alpha \leq max$, $V_{\rm rot}\sin i = 76 - 138$ km s^{-1} and $K_1 = 90 - 113$ km s^{-1}. The shaded area indicates the region allowed by our constraints, which yields $q = 0.21 - 0.34$ and $K_2 = 286 - 433$ km s^{-1}. These imply a mass function $f(M) = M_1 \sin^3 i/(1+q)^2 = 0.76 \pm 0.47$ M$_\odot$ and hence $M_1 \sin^3 i = 1.24 \pm 0.77$ M$_\odot$. Clearly the large uncertainties are dominated by the error in $K_{\rm em}$ and the uncertainty in the disc flaring angle.

6.2 System Parameters for V926 Sco

The same reasoning can be applied to V926 Sco. The spot in the NIII λ4640 map yields $K_{\rm em} = 226 \pm 22$ km s^{-1} whereas the ZAMS Mass-Radius relation for a 4.65 hr Roche lobe leads to $M_2 \leq 0.58 M_\odot$ (Tout et al. 1996) and hence $q \leq 0.41$. On the other hand, we measure $FWHM(NIII\lambda4640) = 115 \pm 23$ km s^{-1} which, after deconvolution of the instrumental resolution using Gray rotation profiles as above, yields $V_{\rm rot}\sin i \geq 71 \pm 21$ km s^{-1}. This lower limit, combined with the $K-correction$ for $\alpha > 0^\circ$ and equation (3), yields $q \geq 0.05$ and, hence $i \leq 80^\circ$. And, under the assumption that the donor star is more evolved than a ZAMS star, the Roche lobe geometry implies $R_2 \leq 0.54 R_\odot$ which, for $i \leq 80^\circ$, leads to $V_{\rm rot}\sin i \leq 137$ km s^{-1}.

All these restrictions translate into constraints on the $K_2 - q$ plane which are presented in Fig. 10. The allowed region results in $q = 0.05 - 0.41$ and $K_2 = 215 - 381$ km s^{-1}, depending on the value of α. These numbers imply $f(M) = 0.53 \pm 0.44$ M$_\odot$ and,

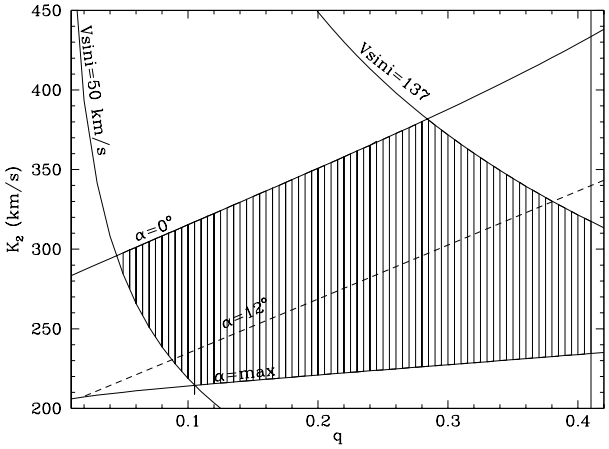

Figure 10. Same as Fig. 9 but for V926 Sco, but with no pulsation constraints yet.

Table 2. System Parameters. T_0 indicates zero phase or inferior conjunction of the donor star. Orbital periods $P_{\rm orb}$ are from G02 and A98.

Parameter	*4U 1636-536* *V801 Ara*	*4U 1735-444* *V926 Sco*
$P_{\rm orb}$ (days)	0.15804693(16)	0.19383351(32)
T_0 (HJD−2 452 000)	813.531 ± 0.002	813.495 ± 0.003
γ (km s^{-1})	-34 ± 5	-140 ± 3
$K_{\rm em}$ (km s^{-1})	277 ± 22	226 ± 22
q (M_2/M_1)	0.21-0.34	0.05-0.41
K_1 (km s^{-1})	90-113	—
K_2 (km s^{-1})	360 ± 74	298 ± 83
$f(M)$ (M$_\odot$)	0.76 ± 0.47	0.53 ± 0.44
i (deg)	36-60	27-60

thus, $M_1 \sin^3 i = 0.80 \pm 0.71$ M$_\odot$. Unfortunately we do not have any contraints on K_1 from burst oscillations and hence our mass restrictions are not as well constrained as for V801 Ara. Our best estimates of the system parameters for both objects are presented in Table 2.

6.3 Constraints on the inclination

Further constraints on the stellar masses requires a knowledge of the binary inclination. While strict upper limits are set by the absence of X-ray eclipses, lower limits can be established by combining $M_1 \leq 3.1$ M$_\odot$ (the maximum mass allowed for a stable neutron star, Rhoades & Ruffini 1974) with our mass function and q restrictions. This leads to $i = 36^\circ - 74^\circ$ and $i = 27^\circ - 80^\circ$ for V801 Ara and V926 Sco, respectively. In addition, the physical model of Frank, King & Lasota (1987) indicates $i \leq 60^\circ$ due to the lack of X-ray dips.

On the other hand, we mentioned in Section 3 that the factor ∼2 narrowness of the HeII λ4686 profile in V926 Sco with respect to V801 Ara indicates a lower inclination. To test this hypothesis we have produced Doppler corrected averages for V801 Ara and V926 Sco by coadding all the spectra in two bins centered at orbital phases 0.0 and 0.5, when the visibility of the irradiated face of the donor is minimum and maximum, respectively. These spectra are presented in Fig. 11 and show a marked difference for the two binaries: the narrow CIII/NIII lines become significantly enhanced around phase 0.5 (top spectra) for V801 Ara, but not much difference is seen in V926 Sco between phase 0.5 and phase 0. This clearly supports a higher inclination angle in V801 Ara. Furthermore, the relative contibution of the NIII λ4640 line with respect to the broad base, as estimated through a multigaussian fit, is a factor ~ 2 larger for V801 Ara than for V926 Sco. This can be taken as the relative contributions of the heated donor and disc, and hence, strongly suggests that V801 Ara is seen at a higher inclination angle than V926 Sco. This seems at odds with the fact that the optical lightcurves in V801 Ara and V926 Sco display similar amplitudes, $A \simeq 0.2$ mags (van Amerongen et al. 1987, van Paradijs et al. 1990). However, de Jong et al. (1996) have shown that lightcurve amplitudes are more sensitive to α than i, which might simply imply a thicker disc in V926 Sco and hence lightcurve amplitudes cannot be taken as a simple indication of the inclination angle.

6.4 Mass Estimate and Evolutionary Scenarios

Meyer & Meyer-Hofmeister (1982) analyzed the effects of X-ray heating in the vertical structure of discs and demonstrated that these are strongly correlated. Even in the absence of irradiation, they find a disc opening angle of $\sim 6^\circ$. De Jong et al. (1996) modelled the effects of irradiation in optical lightcurves and, by comparing with observations of LMXBS, they infer a mean disc opening angle of 12°. Most of their systems are short period LMXBs, just like V801 Ara and V926 Sco, and hence it seems justified to speculate what our system parameters would be in this particular case.

Regarding V801 Ara, $\alpha = 12^\circ$ leads to $q \simeq 0.25 - 0.30$, $K_2 \simeq 356 - 375$ km s^{-1} (see dashed line in Fig. 9) and hence $f(M) \simeq 0.81 \pm 0.07$ M$_\odot$ and $M_1 \sin^3 i \simeq 1.32 \pm 0.13$ M$_\odot$. Asssuming that the donor star is a 0.48 M$_\odot$ ZAMS, then $M_1 \simeq 1.6 - 1.9$ M$_\odot$ and $i \simeq 60 - 71^\circ$. On the other hand, a canonical 1.4 M$_\odot$ would imply an evolved donor with $M_2 \simeq 0.35 - 0.42$ M$_\odot$ and $i \geq 71^\circ$, which is difficult to reconcile with the absence of X-ray eclipses, dips and the low amplitude of the optical modulation (see Sect. 6.3). Therefore, a flaring angle of $\alpha \simeq 12^\circ$ seems to support scenarios with ZAMS donors and massive neutron stars. These masses can be reproduced by recent evolutionary scenarios where some LMXBs are suposed to descend from binaries with high mass donors (Schenker & King 2002). These are significantly evolved at the begining of the mass transfer phase and mass is transferred in a thermal timescale until mass ratio reverses, which can result in the accretion of several tenths solar masses by the neutron star. This would make V801 Ara similar to other LMXBs such as 4U 1822-371 (Muñoz-Darias et al. 2005).

However, it is also possible to accommodate a canonical neutron star with a MS donor and a plausible inclination angle by pushing the disc flaring angle to higher values. For instance, $\alpha = 16^\circ$ leads to $q \simeq 0.30 - 0.34$, $f(M) \simeq 0.51$ M$_\odot$ and $M_1 \sin^3 i \simeq 0.88$ M$_\odot$. Then, for $M_1 = 1.4$ M$_\odot$, $M_2 \simeq 0.45$ M$_\odot$ and $i \simeq 57^\circ$. These masses would be consistent with standard evolutionary pictures where donors in LMXBs descend from slightly evolved low-mass stars through dynamically stable mass transfer and result in slightly undermassive stars.

Note also that $\alpha < 12^\circ$ are virtually ruled out because this would imply higher K_2 and $f(M)$ values which result in massive neutron stars and very high inclinations. For instance, $\alpha = 8^\circ$ leads to $f(M) \simeq 0.96$ M$_\odot$ and $M_1 \sin^3 i \simeq 1.5$ M$_\odot$. Then, for $i \leq 76^\circ$ (lack of X-ray eclipses), $M_1 \geq 1.7$ M$_\odot$ whereas a plaussible $i \simeq 57^\circ$ yields $M_1 \simeq 2.6$ M$_\odot$.

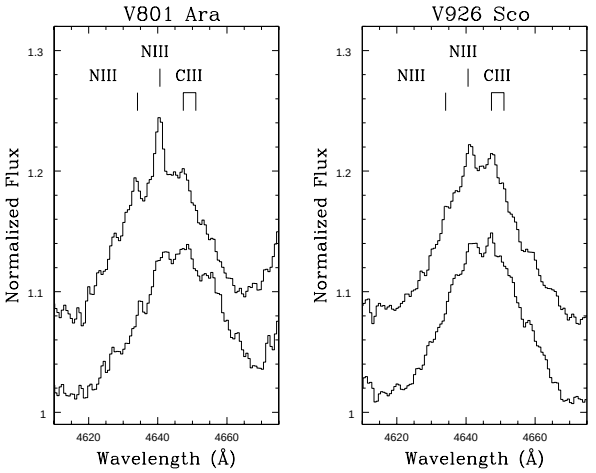

Figure 11. Doppler corrected averages of V801 Ara (left panel) and V926 Sco (right panel) in the rest frame of the donor star. Top spectra present averages between orbital phases 0.25-0.75 and bottom spectra between 0.75-0.25. The sharp CIII/NIII components in V801 Ara are clearly more intense around phase 0.5 than 0, suggesting a higher inclination binary. Spectra have been smoothed by a 2 pixel boxcar.

The case of V926 Sco is unfortunately unconstrained because of the lack of an X-ray mass function. For example, assuming $\alpha = 12^\circ$ leads to $q \simeq 0.09 - -0.38$, $f(M) \simeq 0.22 - -0.68$ $M_\odot$ and $M_1 \sin^3 i \simeq 0.29 - -1.07$ $M_\odot$. The allowed range in M_1 and M_2 is too wide as to impose any useful restriction on possible evoultionary scenarios. More, higher resolution data are required to measure the NIII λ4640 flux and $V_{\rm rot} \sin i$ as a function of orbital phase, from which tighter constraints on the inclination and disc flaring angle can be set. This, together with the determination of the X-ray mass function for V926 Sco through pulse delays of burst oscillations and smaller errors in the $K_{\rm em}$ determinations, is expected to provide stronger limits on the stellar masses and the evolutionary models for these two LMXBs (see e.g. Muñoz-Darias et al. 2005).

7 CONCLUSIONS

The main results of the paper are summarized as follows:

- We have presented the first detection of the donor stars in the bursters LMXBs V801 Ara (=4U 1636-536) and V926 Sco (=4U 1735-444) through NIII λ4640 fluorescent emission caused by irradiation.
- The narrow NIII λ4640 spots in the Doppler maps define $K_{\rm em} = 277 \pm 22$ km s^{-1} (V801 Ara) and $K_{\rm em} = 226 \pm 22$ km s^{-1} (V926 Sco), and a new set of *spectroscopic* ephemerides which lend support to the assumption that photometric modulation is driven by the visibility of the irradiated donor stars. On the other hand, the phasing of the radial velocity curves of HeII λ4684 and the Bowen blend suggest that these lines are mainly associated with the disc bulge. Our spectroscopic ephemerides, combined with burst oscillations data for V801 Ara, enables us to refine the neutron star's projected velocity to $K_1 = 90 - 113$ km s^{-1} for this particular system.
- Following Muñoz-Darias et al. (2005), we have computed the $K - corrections$ for the two LMXBs and obtain $K_2 = 360 \pm 74$ km s^{-1}, $q = 0.21 - 0.34$, $f(M) = 0.76 \pm 0.47$ $M_\odot$ (V801 Ara) and $K_2 = 298 \pm 83$ km s^{-1}, $q = 0.05 - 0.41$, $f(M) = 0.53 \pm 0.44$ $M_\odot$ (V926 Sco). Both systems are seen at intermediate inclination angles in the range $i \simeq 30 - 60^\circ$, with V801 Ara having the higher inclination of the two.
- Regarding V801 Ara, disc flaring angles $\alpha \leq 8^\circ$ seem to be ruled out because of the high inclinations implied. Opening angles $\alpha \simeq 12^\circ$ support massive neutron stars and main-sequence donors which may descend from intermediate-mass X-ray binaries as predicted by some evolutionary models (Schenker & King 2002). Alternatively, higher opening angles $\alpha \simeq 16^\circ$ are consistent with canonical neutron stars and main-sequence (or slightly evolved) donors which have evolved from standard LMXBs through a dynamically stable mass tranfer phase.
- The lack of an X-ray mass function in V926 Sco prevents to set tighter constraints to the $K - correction$, mass estimates and evolutionary history in this LMXB.

ACKNOWLEDGMENTS

We thank the referee Thomas Augusteijn for helful comments to the manuscript. MOLLY and DOPPLER software developed by T.R. Marsh is gratefully acknowledged. JC acknowledges support from the Spanish Ministry of Science and Technology through the project AYA2002-03570. DS acknowledges a Smithsonian Astrophysical Observatory Clay Fellowship as well as support through NASA GO grants NNG04GG96G and NNG04G014G. Based on data collected at the European Southern Observatory, Monte Paranal, Chile.

REFERENCES

van Amerongen S., Pedersen H., van Paradijs J., 1987, A&A, 185, 147
Augusteijn T., van der Hooft F., de Jong J.A.., van Kerkwijk M.H., van Paradijs J., 1998, A&A, 332, 561 (A98)
Casares J., Steeghs D., Hynes R.I., Charles P.A., O'Brien K., 2003, ApJ, 590, 1041
Corbet R.H.D., Thorstensen J.R., Charles P.A., Menzies J.W., Naylor T., Smale A.P., 1986, MNRAS, 222, 15P
Cornelisse R., Steeghs D., Casares J., Barnes A.D., Charles P.A., Hynes R.I., O'Brien K., 2006, MNRAS, submitted
Cowley A.P., Crampton D., Hutchings J.B., 1882, ApJ, 255, 596
Frank, J., King A.R., Lasota J.-P., 1987, A&A, 178, 137
Galloway D.K., Psaltis D., Muno M.P., Chakrabarty D., 2005, ApJ, in press, astro-ph/05113801
Giles A.B., Hill K.M., Strohmayer T.E., Cumming N., 2002, ApJ, 568, 279 (G02)
Gray D.F., 1992, "The observation and Analysis of Stellar Photospheres", CUP 20
Hasinger G., van der Klis M., 1989, A&A, 225, 79
Haswell C.A., King A.R., Murray J.R., Charles P.A., 2001, MNRAS, 321, 475
Hellier C., Mason K.O., 1989, MNRAS, 239, 715
Horne K., 1986, PASP, 98, 609
Hynes R.I., Steeghs D., Casares J., Charles P. A., O'Brien K., 2003, ApJ, 583, L95
de Jong J.A., van Paradijs J., Augusteijn T., 1996, A&A, 314, 484
Marsh T.R., 1998, in Wild Stars in the Old West, eds. S. Howell, E. Kuulkerss and C. Woodward (ASP Conf. Series) vol. 137, p.236
Marsh T.R., 2001, in Astrotomography, Indirect Imaging Methods in Observational Astronomy, eds. H.M.J. Boffin, D. Steeghs and J. Cuypers (Lecture Notes in Physics) vol. 573, p.1

Meyer F., Meyer-Hofmeister E., 1982, A&A, 106, 34
McClintock J.E., Canizares C., Tarter C.B., 1975, ApJ, 198, 641
Muñoz-Darias T., Casares J., Martínez-Pais, I.G., 2005, ApJ, 635, 502
Nakanishi H., Sofue Y., 2003, PASJ, 55, 191
Nussbaumer H., 1971, ApJ, 170, 93
Paczynski B., 1971, Ann. Rev. A&A, 9, 183
van Paradijs J., van der Klis M., Pedersen H., 1988, A&A, 76, 185
van Paradijs J. et al., 1990, A&A, 234, 181
van Paradijs J., McClintock J. E., 1995, in X-ray Binaries,Cambridge Astrophysics Series: Cambridge University Press. eds. W.H.G. Lewin, J. van Paradijs & E.P.J. van den Heuvel, p. 58
Pedersen H., van Paradijs J., Lewin W.H.G., 1981, Nature, 294, 725
Rhoades C.E., Ruffini R., 1974, Phys. Rev. Lett., 32, 324
Shafter A.W., Szkody P., Thorstensen J.R., 1986, ApJ, 308, 765
Schachter J., Filippenko A.V., Kahn S.M., 1989, ApJ, 340, 1049
Schenker K., King A.R., 2002, ASP Conf. Ser. 261: The Physics of Cataclysmic Variables and Related Objects, 261, 242
Schneider D.P., Young P., 1980, ApJ, 238, 946
Smith D.A., Dhillon V.S., 1998, MNRAS, 301, 767
Steeghs D., Casares J., 2002, ApJ, 568, 273 (SC02)
Strohmayer T.E., Zhang W., Swank J.H., White N.E., Lapidus I., 1998, ApJ, 498, L135
Strohmayer T.E., Markwardt C.B., 2002, ApJ, 577, 337 (SM02)
Strohmayer T.E., Bildsten L., 2004, in X-ray Binaries, Cambridge Astrophysics Series: Cambridge University Press. 2004. eds. W.H.G. Lewin & M. van der Klis.
Smale A.P., Corbet R.H.D., 1991, ApJ, 383, 853
Tout C.A., Pols O.R., Eggleton P.P., Zhanwen H., 1996, MNRAS, 281, 257
Wade R.A., Horne, K., 1988, ApJ, 324, 411
Warner B., 1995, ApJ&SS, 232, 89

This paper has been typeset from a TEX/ LATEX file prepared by the author.